http://www.press.ierek.com

ISSN (Print: 2357-0849, online: 2357-0857)

Environmental Science and Sustainable Development

Research Paper

Received: 24 April 2025, Accepted:07 August 2025, Published online: 31 December 2025

DOI: 10.21625/essd.v10i4.1211

Topology Optimization of Horizontal Links in Multi-story Eccentric Braced Frames

Amr M. Ibrahim[1]*, Ahmed Ashraf[2], Yasser N. Saleh[3]

[1]*Assistant Professor, Civil Engineering Department, The British University in Egypt, Cairo, Egypt*

[2]*Undergraduate student, Civil Engineering Department, The British University in Egypt, Cairo, Egypt*

[3]*Assistant Lecturer, Civil Engineering Department, The British University in Egypt, Cairo, Egypt*

Abstract

In recent years, the adoption of additive manufacturing has become important, primarily driven by an imperative to minimize material usage and mitigate environmental impacts associated with climate change. The integration of topology optimization and additive manufacturing techniques has paved the way for the fabrication of complex geometries that are both ***cost-effective*** and material efficient, enabling structures that would be challenging to produce using traditional manufacturing methods. Concurrently, the application of eccentric braced frames with link elements has seen a notable increase, attributed to their enhanced seismic resistance capabilities compared to concentric braced frames. This study integrates topology optimization and AM to design optimized shear links for EBFs that outperform standard HEB European sections. Finite Element Models were developed in Abaqus to simulate both monotonic and cyclic loading scenarios. Pushover and cyclic analyses were performed on single-, two-, and three-story frames to assess the performance of the optimized links. Through pushover analysis, the results show that employing optimized HEB sections leads to a significant reduction in steel volume while simultaneously enhancing both the yielding and ultimate strength of the structure, with some multi-story frames demonstrating a twofold increase in performance over standard designs. Moreover, cyclic performance analysis of models with optimized links underscores a notable increase in the base shear ultimate force with marked improvement in the effective stiffness compared to models with standard sections. However, this was accompanied by a reduction in energy dissipation and the viscous damping coefficient.

Keywords

Eccentrically braced frames; Shear link; Topology optimization; Pushover analysis; Cyclic loading.

1. Introduction

The inclusion of additive manufacturing (AM) offers a transformative shift in the construction and structural engineering industries, presenting significant potential for innovation, optimization, and sustainability. AM allows the production of complex geometries directly from digital models (Bos et al., 2016), significantly expanding the design space available to engineers and architects. In particular, Wire and Arc Additive Manufacturing (WAAM) has gained traction as a viable method for large-scale structural fabrication due to its high deposition rate, geometric flexibility, and cost-effectiveness (Shukla et al., 2020). The integration between AM and topology optimization made

a generation of optimized structures with efficient material distribution possible with the aid of finite element applications (Craveiro et al. 2017). The use of AM in construction enables the production of unique components that are difficult to fabricate using traditional techniques (Labonnote et al., 2016). Recent high-profile applications—such as the Gaudí-inspired pavilion in Barcelona, Spain, and the 3D-printed office buildings in Dubai—demonstrate the architectural and structural capabilities of AM in producing complex forms that would be challenging, if not impossible, to achieve through conventional manufacturing methods (Lange et al., 2021).

This advancement aligns naturally with the field of topology optimization, a computational design approach that strategically redistributes material within a given domain to achieve maximum structural performance with minimum material use. Topology optimization, particularly using methods like Solid Isotropic Material with Penalization (SIMP), has proven effective in generating lightweight and structurally efficient components, often with non-intuitive geometries that require AM for physical realization (Bendsøe & Sigmund 2013; Galjaard et al., 2014). Previous studies have extended this methodology to various structural elements, including perforated beams (Tsavdaridis et al., 2015), trusses, and custom joints, with demonstrated benefits in both mechanical performance and material sustainability. The integration of AM with topology optimization not only enables highly efficient load paths but also supports sustainability goals by reducing material waste and embodied carbon in construction (Craveiro et al., 2017; Wu et al., 2016).

In the context of seismic design, the application of topology optimization remains relatively underexplored but increasingly important. One of the most promising structural systems in seismic regions is the Eccentrically Braced Frame (EBF), which combines the ductility of moment-resisting frames with the stiffness and strength of concentrically braced frames. Central to the performance of EBFs is the shear link, a designated yielding component that dissipates energy during seismic events and protects the main structural members from inelastic deformation (Della Corte et al., 2013; Bruneau et al., 2011). Conventional shear links are typically fabricated from rolled steel profiles such as HEB sections, chosen for their availability and standardized behavior. However, these standard profiles do not necessarily represent the most material-efficient or performance-optimized solutions, particularly in complex or high-seismic applications.

Recent research efforts have begun exploring the potential of topology-optimized shear links to improve the performance of EBFs. Notably, Ramonell and Chacón (2021) employed ABAQUS-based finite element modeling to design and assess topology-optimized horizontal links, reporting improvements in both yielding and ultimate strength compared to standard HEB sections. Similarly, Saleh et al. (2024) extended this work to vertical shear links and cyclic loading conditions, further demonstrating the viability of optimization for enhancing seismic performance. These studies collectively highlight the potential of combining AM and topology optimization to create next-generation structural components that are both efficient and resilient.

However, the majority of existing research has focused on single-story frames, which do not fully capture the structural complexity or interaction effects present in multi-story buildings. As seismic demands and inter-story drift accumulate over height, the behavior of optimized shear links may differ significantly, necessitating further investigation into their scalability and effectiveness in multi-story contexts. This study aims to extend the current state of knowledge by applying topology optimization to horizontal shear links in multi-story EBFs and evaluating their performance under both monotonic (pushover) and cyclic loading conditions. Finite element models developed in Abaqus are used to simulate realistic boundary conditions and loading protocols, with performance metrics including base shear capacity, effective stiffness, energy dissipation, and buckling behavior. Comparisons between conventional HEB sections and their topology-optimized counterparts are made across one-, two-, and three-story frame configurations. This research also seeks to reduce structural material usage through computational topology optimization, thereby achieving volume-efficient structural components with improved seismic performance. This volume reduction directly translates into a lower demand for steel, which contributes to minimizing resource consumption and embodied carbon emissions—two core themes in environmental sustainability. As the steel industry is a major contributor to global CO_2 emissions, designing structural elements that require less material promotes more sustainable construction practices. In doing so, this research seeks to not only demonstrate the potential benefits of

topology-optimized shear links in seismic design but also identify the limitations and considerations that must be addressed for their broader implementation.

2. Numerical Modeling

Finite Element Models (FEM) within Abaqus were deployed to conduct pushover analyses on horizontal links in eccentric braced frames. The specifications of the link sections, including dimensions and material properties, were directly sourced from (Ramonell & Chacón, 2021), facilitating a rigorous validation of the resultant data. The sections utilized in this study are detailed in Table 1, with the material of choice being European steel grade S275. The material's plastic behavior is characterized by a nonlinear profile, delineated through two critical points: an initial yield point at zero strain and an ultimate strength of 430 MPa at a maximum strain of 0.2. The geometry and dimensions of the eccentric braced frame under investigation are illustrated in Figure 1. For this analysis, the entire frame is modeled using wire elements, whereas the link component is designated as a solid element to facilitate focused study.

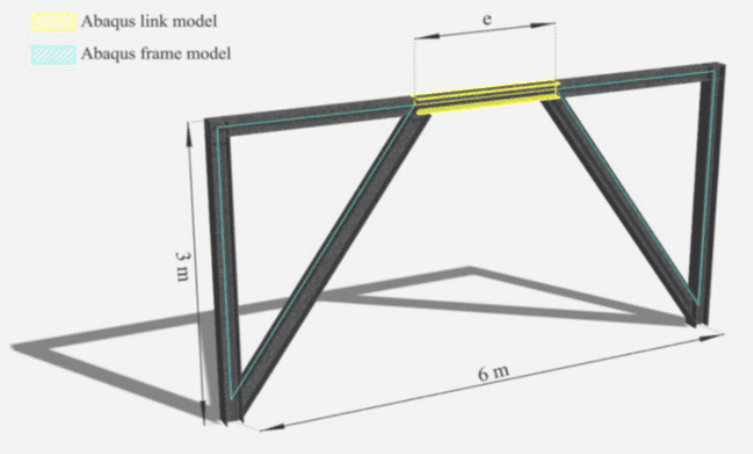

Figure 1. Eccentric braced frame dimensions (source: Ramonell & Chacón, 2021)

Table 1. Eccentric braced frame sections (source: Ramonell & Chacón, 2021).

Model	Link section	Beam section	Diagonal section	Column section	Link length (e) (m)
1	HEB140	HEB140	HEB200	HEB180	0.75
2	HEB160	HEB160	HEB200	HEB200	0.83
3	HEB180	HEB180	HEB200	HEB200	0.93

2.1. Mesh Convergence

To ensure the utmost accuracy of results for each link, the frame underwent meshing with a specified size of 10 mm, employing a linear beam in spatial configuration with two nodes (B31), aligning with the default setting for wire elements. The selection of a 10 mm mesh was substantiated through an analysis of the forces at a displacement of 56 mm across varying mesh sizes. It was observed that results stabilized at a mesh size of 10 mm, with the discrepancy between mesh sizes of 10 mm and 100 mm being a negligible 0.00155233%. This analysis conclusively validates the suitability of a 10 mm mesh for all three models, affirming its non-impact on the integrity of the results.

For all link analyses, the mesh was standardized using the hexahedral linear element with reduced integration from the Abaqus library (C3D8R). Initial trials with various mesh sizes for the HEB140 link yielded unstable results, underscoring the necessity of a comprehensive mesh convergence study. Such an investigation is paramount to ascertain the optimal mesh size that ensures stability and accuracy across all link models. The findings from the mesh

convergence analysis indicated that a mesh size of 9 mm was most conducive to convergence for both HEB140 and HEB160 links. Conversely, for the HEB180 link, stability was achieved with a mesh size of 10 mm or larger.

2.2. Boundary Conditions

To preclude any out-of-plane movements within the eccentric braced frame, the columns and beams were externally constrained by restricting the U3 displacement, effectively immobilizing them in the out-of-plane direction. Furthermore, the frame's base points were configured as pinned, ensuring rotational freedom while preventing translational movements. Additionally, to facilitate the pushover analysis, a target displacement of 56 mm was applied at the frame's eave as shown in Figure 2. Ramonell & Chacón (2021) advocate for the implementation of a coupling constraint to preserve the kinematic coupling between the link and the frame as illustrated in Figure 3, thereby enhancing the solution's accuracy with respect to degrees of freedom. This coupling is strategically applied between a designated point on the frame and the corresponding surface of the link.

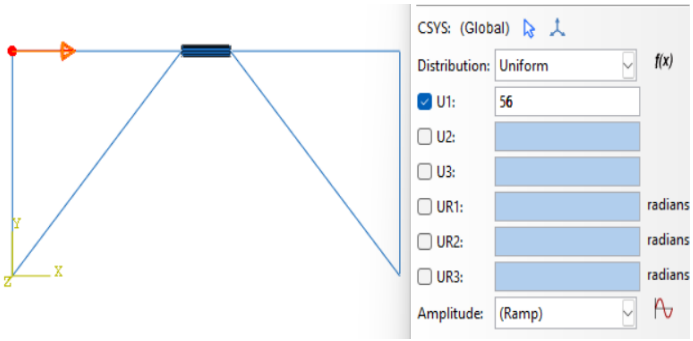

Figure 2. Assigned displacement for pushover analysis (source: by authors)

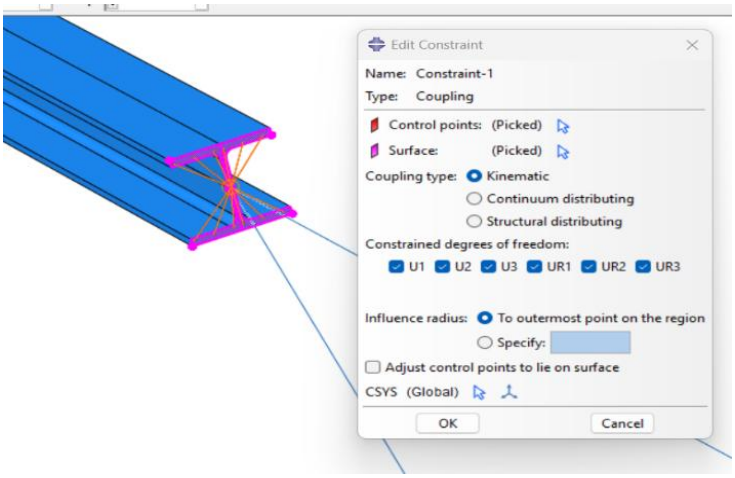

Figure 3. Coupling constraint between the solid element model of the link and the frame elements representing the rest of the EBF model (source: by authors)

2.3. Topology Optimization Method

The conventional HEB profile is substituted with a cubic volume, mirroring the dimensions, width, depth, and length of the HEB originally employed, as depicted in Figure 4. In the pursuit of mesh convergence, varying mesh sizes were evaluated through topology optimization for the HEB 140 model. A pushover analysis utilizing the cubic link model facilitated the generation of force-displacement curves, alongside correlations between the number of elements and forces at a 56mm displacement. Interestingly, the results indicated uniformity across different mesh sizes, a phenomenon attributable to the geometric simplicity of the cubic shape, rendering mesh size a non-critical factor in this context. Conversely, stress distribution within the optimized shape varied significantly across different meshes. This variability underscores the influence of mesh size on stress distribution outcomes within the topology optimization process. Specifically, for meshes sized 10mm and 15mm, minimal stress was observed in the initial third of the shape. Meanwhile, a 5mm mesh size resulted in stress concentration within the link's central region. This

observation highlights how mesh granularity affects stress distribution across the link, corroborating Ramonell & Chacón (2021) assertion that finer meshes yield more detailed shape resolutions, thereby enhancing the scope for material reduction during topology optimization. Consequently, a 10mm mesh size was selected for all topology-optimized links, aiming to centralize stress distribution within the link to optimize computational efficiency in subsequent topology optimization iterations.

The optimization process was refined by adjusting the increment settings to medium, initiating with zero percent initial material removal. Central to this methodology is the establishment of two singular term responses derived from the comprehensive response list: 1) Strain energy encompassing the entire model, and 2) Volume pertaining to the link area targeted for topology optimization. The primary objective function concerning strain energy aims to maximize the design's overall response. Concurrently, a volume design response criterion facilitates the desired material reduction in the link area by approximately 18%, aligning the optimized link volume closely with that of traditional HEB section volumes. This strategy is graphically represented in Figure 5.

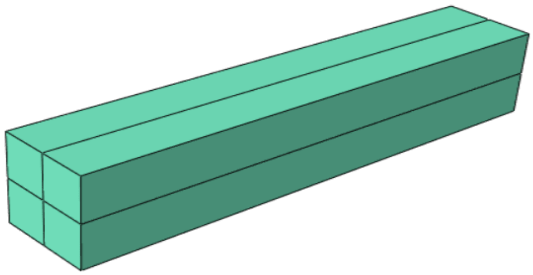

Figure 4. Link used for topology optimization (source: by authors)

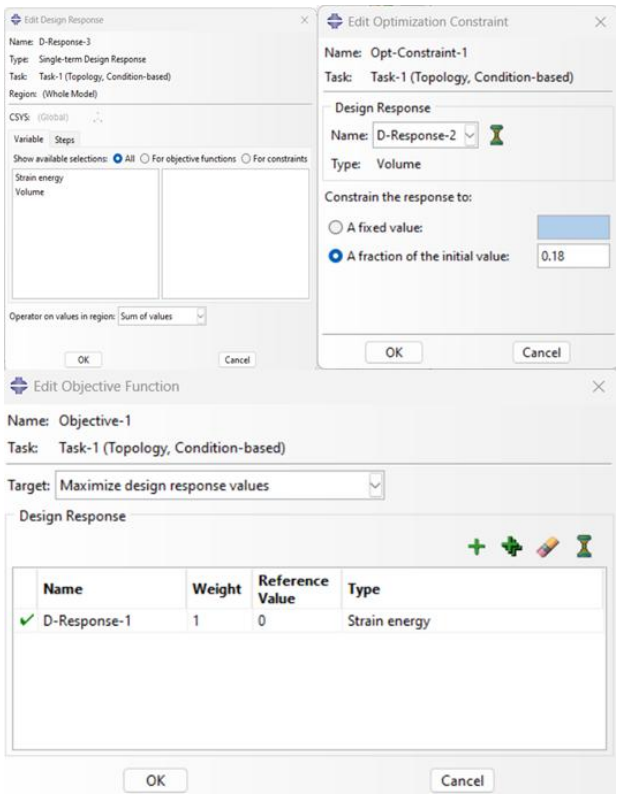

Figure 5. Topology optimization procedure *(source: by authors)*

Following the completion of the topology optimization process, the optimized shape was extracted as an Abaqus input (.inp) file, located within the topology optimization job directory. This crucial step facilitates the integration of the optimized shape into the model, a process visually depicted in Figure 6. Subsequently, a crucial modification of the mesh configuration was undertaken, transitioning from triangular (tri) to tetrahedral (tet) elements. This

transformation is essential for converting the optimized shape from a shell to a solid element format, thereby enabling the assignment of material properties to the newly optimized shape. The assembly of the model was facilitated by incorporating the obtained part instance into the assembly environment. This instance was automatically positioned at the specific location extracted from the optimization output, streamlining the integration of the topology-optimized component within the overall model framework. Subsequent to the assembly, kinematic coupling was established to maintain the structural integrity and functional interaction between the frame and the optimized link. This was achieved by selecting the entire surface of the optimized shape as the coupling region, effectively linking the control points of the frame to the surface of the optimized link.

Figure 6. Sample of the extracted optimized shapes (source: by authors)

2.4. Multi-story EBF

To model multi-story Eccentric Braced Frames (EBFs), the initial single-story model underwent duplication one or two times, thereby generating structures with two or three stories, respectively. In ensuring structural integrity and preventing out-of-plane movements, the beams and columns of the newly added frames were rigidly fixed. Additionally, to maintain the structural and functional coherence between the link and the frame across all stories, kinematic coupling was systematically applied. Consistent with the single-story model, a displacement of 56mm was imposed at the top corner of the EBF for each story, ensuring uniformity in the simulation parameters. The methodology for topology optimization was adapted for the multi-story context by introducing a cubic volume in the story designated for optimization, while retaining normal HEB links in the remaining stories. The validation of the optimized link was conducted through a comparative analysis between the results obtained by Ramonell & Chacón (2021) and those derived from the HEB 160 model. This comparative evaluation is graphically represented in Figure 7, demonstrating a congruence between the results. Such identical outcomes affirm the reliability and accuracy of the developed model.

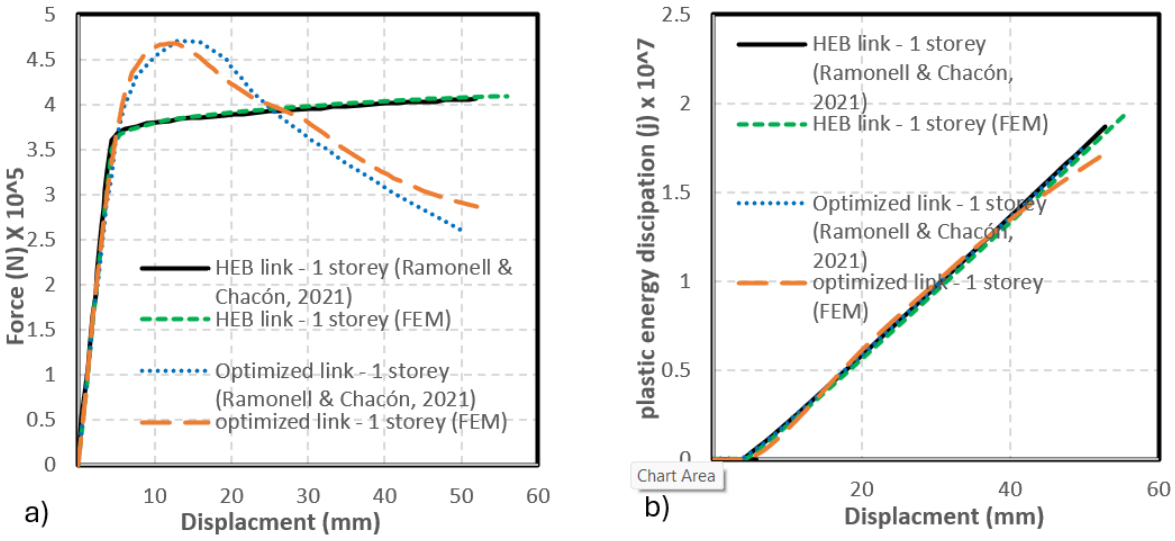

Figure 7. Validation for HEB and optimized links: a) force, displacement, b) plastic energy dissipation – displacement (source: by authors)

3. Pushover Analysis

The pushover analysis, conducted on each optimized link, was meticulously compared with the performance metrics of the conventional HEB links to evaluate enhancements or modifications in structural behavior. Notably, the analysis revealed that the performance improvements attributed to the optimized links were more pronounced in structures comprising two and three stories than in single-story configurations. This observation is particularly evident in the force-displacement curves, where, for single-story applications, the curves of optimized links closely approximated those of standard HEB sections, indicating a marginal performance differentiation. For the HEB 140 models, the comparative force-displacement curves are illustrated in Figure 8. Furthermore, a comprehensive comparison encapsulating the performance outcomes of both optimized and conventional links is presented in Table 2.

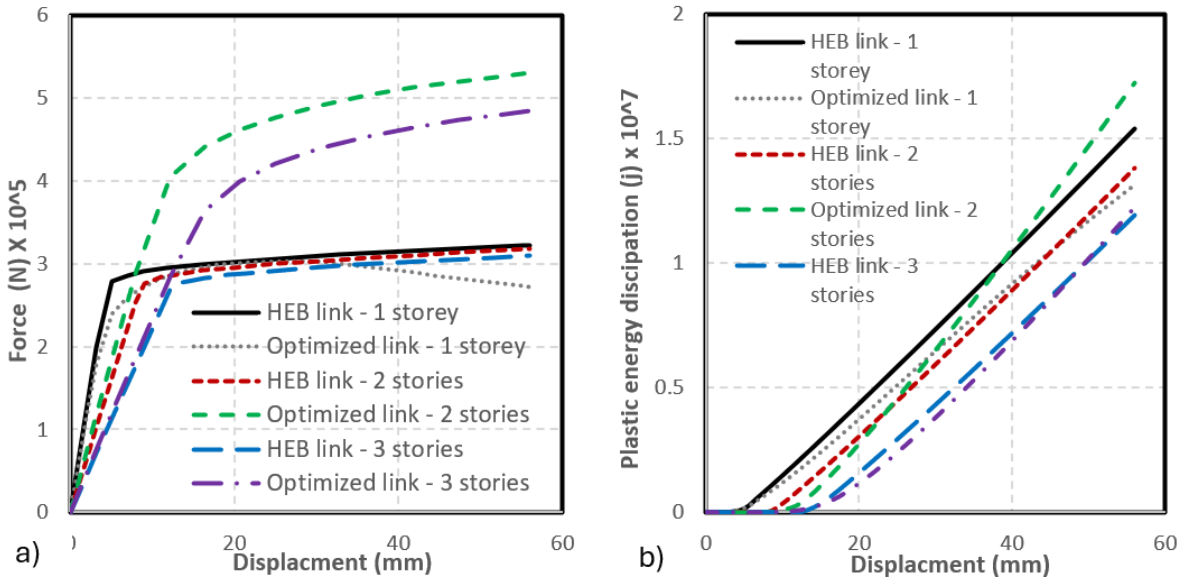

Figure 8. HEB140 pushover analysis results: a) force, displacement, b) plastic energy dissipation – displacement (source: by authors)

Table 2. Pushover analysis results.

Story	Effective yielding (*N*)	%	Yielding displacement (mm)	%	Effective stiffness (N/mm)	%	Volume (mm^3)	%	Max. force (*kN*)	%	Max. energy (*KJ*)	%
HEB 140												
1 HEB	168,000	89.3	2	100.0	84,000	89.3	3,225,000	93.2	322	94.1	15,383	85.3
1 OPT	150,000		2		75,000		3,004,780		303		13,128	
2 HEB	165,000	145.5	6	100.0	27,500	145.5	6,450,000	94.0	317	167.2	13,783	125.1
2 OPT	240,000		6		40,000		6,062,480		530		17,245	
3 HEB	162,000	144.4	8	137.5	20,250	105.1	9,675,000	93.6	309	156.6	11,933	102.5
3 OPT	234,000		11		21,273		9,053,850		484		12,235	
HEB 160												
1 HEB	213,000	123.9	3	100.0	71,000	123.9	4,506,900	100.0	409	114.2	19,587	86.7
1 OPT	264,000		3		88,000		4,505,650		467		16,991	

2 HEB	216,000	166.7	5	160.0	43,200	104.2	9,013,800	99.2	423	179.7	17,717	142.3
2 OPT	360,000		8		45,000		8,938,390		760		25,206	
3 HEB	210,000	157.1	8	150.0	26,250	104.8	13,520,700	97.8	408	173.5	15,265	115.9
3 OPT	330,000		12		27,500		13,223,500		708		17,687	
HEB 180												
1 HEB	260,000	161.5	4	150.0	65,000	107.7	6,138,200	99.9	495	159.4	19,626	168.2
1 OPT	420,000		6		70,000		6,129,870		789		33,013	
2 HEB	264,000	161.4	8	137.5	33,000	117.4	12,276,400	99.2	497	173.0	19,553	115.0
2 OPT	426,000		11		38,727		12,180,200		860		22,483	
3 HEB	258,000	136.8	11	109.1	23,455	125.4	18,414,600	99.5	477	150.9	15,809	94.5
3 OPT	353,000		12		29,417		18,314,469		720		14,938	

4. Applied cyclic loading

The cyclic loading protocol adheres to the specifications outlined in the (AISC, 2016) guidelines, utilizing predefined link rotational angles. These angles are set at 0.0025, 0.005, 0.01, 0.02, 0.03, 0.04, 0.05, 0.06, 0.07, 0.08, and 0.09. The protocol specifies that the first three angles undergo three loading cycles each, while the subsequent angles are subjected to two cycles. This approach ensures that the maximum rotational angle reaches 0.09, accommodating the typical range of shear link rotational angles, noted in the literature as spanning from 0.02 to 0.08. Given the known lengths of the link and the total beam for each model, a ratio—representing the division of the eccentric braced frame's length by the link's length—is calculated. Drift is then determined by dividing the link rotational angle by this ratio. Subsequently, displacement calculations are conducted by multiplying the height of the eccentric braced frame by the derived drift value. Furthermore, within the ABAQUS environment, the material's plastic hardening behavior is adjusted to a kinematic model. For each model, an amplitude is defined to facilitate the execution of the cyclic analysis, ensuring a rigorous and methodologically sound investigation into the structural dynamics of eccentric braced frames under cyclic loading conditions. The cyclic behavior was analyzed by obtaining the base shear for each model. From the base shear, an envelope is made to compare the behavior of the optimized shape and the normal HEB link. The energy dissipation coefficient is calculated using the area under the force-displacement curve and the two triangles OBE and ODF shown in Figure 9. The effective stiffness (k_e) is obtained by knowing the maximum and minimum forces and their corresponding displacements (FEMA 356, 2000), a methodological detail is also illustrated in Fig. 9. The viscous damping coefficient (h_e) is obtained using Eq. 1 as follows:

$$h_e = \frac{1}{2\pi}.\frac{S_{ABC} + S_{ADC}}{S_{BOE} + S_{DOF}} \quad (1)$$

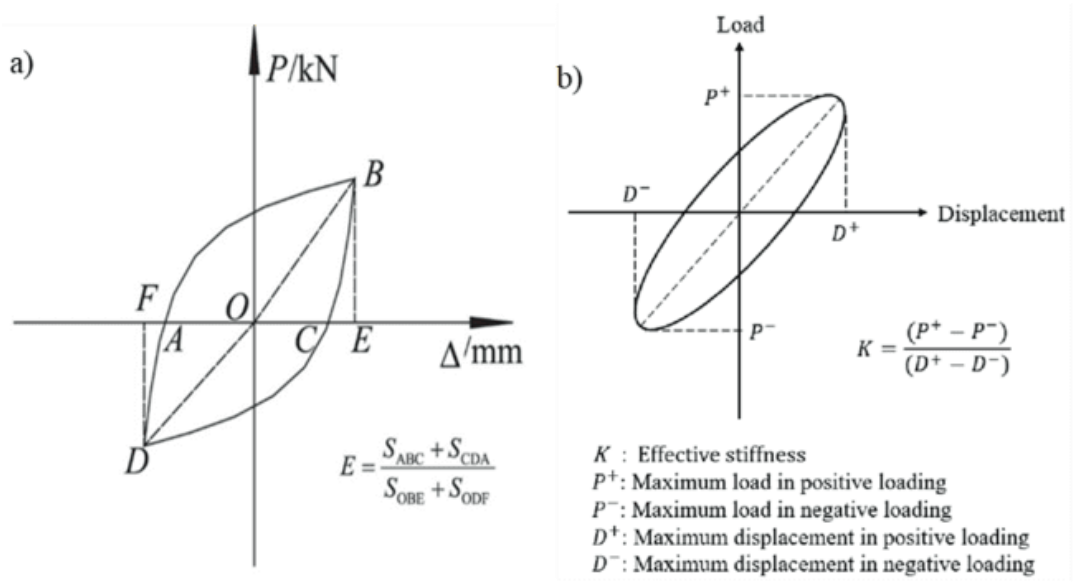

Figure. 9. a) Energy dissipation calculation method (AISC, 2016). b) Effective stiffness method (FEMA 356, 2000).

The results show that while performance metrics such as effective stiffness and base shear capacity improved in optimized links. However, energy dissipation capacity and damping efficiency were reduced. Moreover, The cyclic analysis revealed a notable phenomenon where all optimized links exhibited a buckling effect, predominantly in one direction. This buckling, while not catastrophic, was consistently observed across various frame configurations and indicates a structural vulnerability introduced during the optimization process. The cause can be attributed to the redistribution of material away from regions that contribute to out-of-plane stiffness—a consequence of compliance-based topology optimization that does not inherently account for stability or local buckling resistance. While symmetry is often preserved in standard sections, the freedom allowed in topology optimization to remove material wherever deemed structurally redundant may lead to irregularities that, under dynamic conditions, act as triggers for instability. A sample of the force-displacement results for the HEB 140 links in the 2-storey model, illustrating this behavioral pattern, is graphically represented in Figure 10. Additionally, Table 3 consolidates the comprehensive outcomes derived from the cyclic analysis across all tested models.

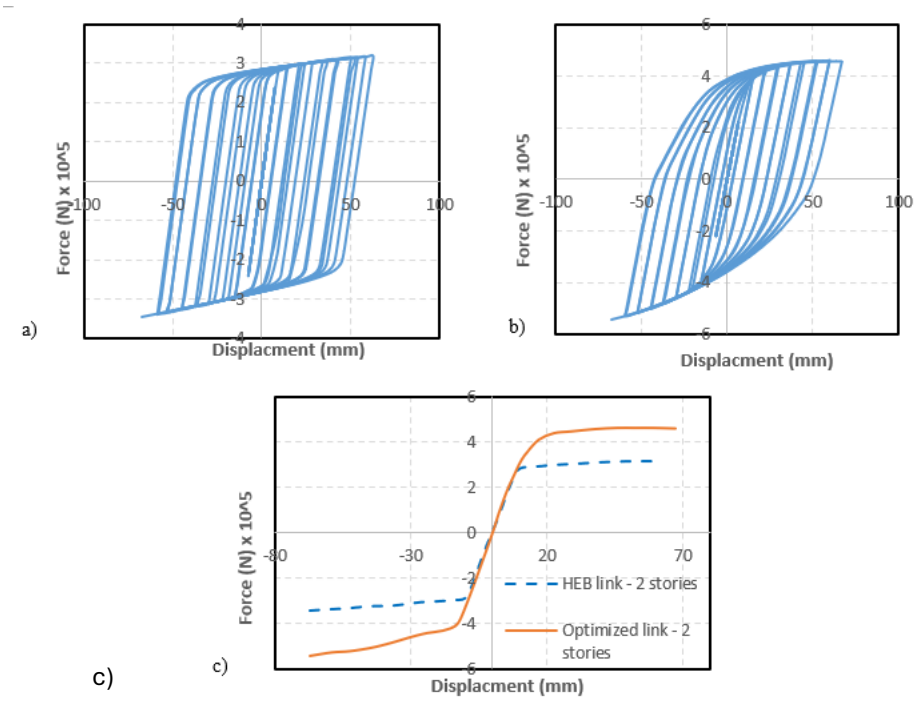

Figure 10. Cyclic Base shear response for (a) HEB 140 link (b) Opt. HEB 140 link (c) cyclic envelope for 2-storey EBF (source: by authors)

Table 3. Cyclic analysis results.

Story	K_e (N/m)	%	Max. force (N)	%	Min. force (N)	%	Energy dissipation	%	h_e	%
HEB 140										
1 HEB	10,302	101.9	307,853	96.7	358,631	114.6	2.855	82.2	0.454	82.3
1 OPT	10,501		297,841		410,882		2.348		0.374	
2 HEB	5,110	145.8	319,126	142.7	346,766	157.3	3.01	75.3	0.489	73.8
2 OPT	7,448		455,458		545,365		2.268		0.361	
3 HEB	3,351	129.6	323,685	109.6	342,450	152.6	2.879	62.7	0.458	62.7
3 OPT	4,342		354,610		522,683		1.806		0.287	
HEB 160										
1 HEB	11,695	174.9	401,947	161.1	465,769	185.7	2.94	65.8	0.468	65.8
1 OPT	20,459		647,607		864,903		1.934		0.308	
2 HEB	5,927	180.3	417,403	171.6	453,089	192.1	2.975	77.9	0.473	78.0
2 OPT	10,689		716,336		870,296		2.319		0.369	
3 HEB	3,942	159.8	422,490	142.1	447,451	181.3	2.949	73.0	0.469	73.0
3 OPT	6,299		600,161		811,064		2.153		0.343	
HEB 180										
1 HEB	12,298	169.5	482,327	163.3	555,358	174.6	2.926	78.7	0.466	78.7
1 OPT	20,845		787,750		969,471		2.302		0.366	
2 HEB	6,378	143.8	497,079	133.0	539,269	164.6	2.873	71.5	0.457	71.5
2 OPT	9,170		661,136		887,603		2.053		0.327	
3 HEB	4,124	126.7	505,639	133.4	532,945	169.1	2.82	68.5	0.45	68.4
3 OPT	5,222		674,760		901,047		1.933		0.308	

5. Conclusions

The integration of additive manufacturing and topology optimization opens new avenues for research, design, and construction of complex steel elements. This synergy promotes the creation of novel, complex structural sections and contributes to material conservation and environmental sustainability. Comparative analysis through pushover analysis between conventional HEB links and their optimized counterparts reveals significant findings. The optimized shapes demonstrate an increase in effective yielding force and a substantial enhancement in the base shear ultimate force across all models, with the sole exception of the HEB 140 one-story model, which closely parallels the performance of the standard HEB link. This enhancement translates into an augmented effective stiffness for the optimized configurations. Furthermore, plastic energy dissipation analysis indicates a comparable performance

between the optimized and conventional HEB links. Cyclic performance analysis of the optimized shapes underscores a notable increase in the base shear ultimate force, reaffirming the structural benefits of the optimization.

Despite the improved stiffness and strength observed in the optimized shear links, the study revealed limitations related to directional buckling and reduced energy dissipation capacity under cyclic loading. These issues highlight the need to explore multi-objective topology optimization that incorporates structural stability requirements, fatigue performance criteria, and energy dissipation capacity. Additionally, experimental validation of the optimized geometries, especially under dynamic loading, is recommended to support practical implementation and improve design robustness.

Acknowledgments

The abstract of this paper was presented at the Environmental Design, Material Science, and Engineering Technologies (EDMSET) Conference - 2nd Edition, which was held on the 22nd - 24th of April 2025.

Funding declaration

The authors would like to acknowledge the British University in Egypt for the travel grant that supported the publication of this document.

Ethics Approval

Not applicable.

Conflict of Interest

The authors declare there is no conflict.

References

Bos, F., Wolfs, R., Ahmed, Z., & Salet, T. (2016). Additive manufacturing of concrete in construction: Potentials and challenges of 3D concrete printing. Virtual and Physical Prototyping, 11(3), 209–225. https://doi.org/10.1080/17452759.2016.1209867

Shukla, P., Dash, B., Kiran, D. V., & Bukkapatnam, S. (2020). Arc behavior in the wire arc additive manufacturing process. Procedia Manufacturing, 48, 725–729. https://doi.org/10.1016/j.promfg.2020.05.105

Craveiro, F., Bartolo, H. M., Gale, A., Duarte, J. P., & Bartolo, P. J. (2017). A design tool for resource-efficient fabrication of 3d-graded structural building components using additive manufacturing. *Automation in Construction*, *82*, 75-83.

Labonnote, N., Rønnquist, A., Manum, B., & Rüther, P. (2016). Additive construction: State-of-the-art, challenges and opportunities. Automation in Construction, 72, 347–366. https://doi.org/10.1016/j.autcon.2016.08.026

Lange, J., Feucht, T., & Erven, M. (2021). 3D-printing with steel – Additive manufacturing connections and structures. CE/Papers, 4(2–4), 2–7. https://doi.org/10.1002/cepa.1258

Bendsøe, M. P., & Sigmund, O. (2013). Topology optimization: Theory, methods, and applications. Springer. https://doi.org/10.1007/978-3-662-05086-6

Galjaard, S., Hofman, S., & Ren, S. (2014). New opportunities to optimize structural designs in metal by using additive manufacturing. In Advances in architectural geometry 2014 (pp. 79-93). Cham: Springer International Publishing.

Tsavdaridis, K. D., Kingman, J. J., & Toropov, V. V. (2015). Application of structural topology optimisation to perforated steel beams. Computers & Structures, 158, 108–123. https://doi.org/10.1016/j.compstruc.2015.05.004

Wu, P., Wang, J., & Wang, X. (2016). A critical review of the use of 3-D printing in the construction industry. Automation in Construction, 68, 21–31. https://doi.org/10.1016/j.autcon.2016.04.005

Della Corte, G., D'Aniello, M., & Landolfo, R. (2013). Analytical and numerical study of plastic overstrength of shear links. Journal of Constructional Steel Research, 82, 19–32. https://doi.org/10.1016/j.jcsr.2012.11.013

Bruneau, M., Uang, C. M., & Sabelli, R. (2011). Ductile design of steel structures (2nd ed.). McGraw-Hill Education.

Ramonell, C., & Chacón, R. (2021). On the topological optimization of horizontal links in eccentrically braced frames. Journal of Constructional Steel Research, 185, 106887. https://doi.org/10.1016/j.jcsr.2021.106887

Saleh, Y. N., Mourad, S. A., & Ibrahim, A. M. (2024, August). Topology optimization of vertical shear links in eccentrically braced frames. Structures, 66, 106821. https://doi.org/10.1016/j.istruc.2024.106821

American Institute of Steel Construction. (2016). Seismic provisions for structural steel buildings (ANSI/AISC 341-16). Chicago, IL.

Federal Emergency Management Agency. (2000). Prestandard and commentary for the seismic rehabilitation of buildings (FEMA 356), Wshington, DC.